

Determination of Anomaly Source Border Using Reweighting Focusing Inversion of Two-Dimensional Gravity Horizontal Gradient Data and Conventional Edge Detection Methods (Case Study: A Chromite Mass in Sabzevar, Iran)

Mahsa Kabiri^{1*} and Zohreh Sadat Riazi Rad²

Abstract

There are numerous methods to detect the edge of gravity and magnetic field anomaly source, most of which are based on the combination of first and second-order horizontal and vertical gradients of the potential field. Gradient-based and other edge detection methods determine the anomaly source borders on the ground surface. In the present study, a linear reweighting focusing inversion method has been used to detect the vertical edges of a subsurface mass using gravity horizontal gradient data. With simultaneous evaluation the results of the proposed method and the conventional edge detection methods, we can accurately detect the subsurface anomaly sources boundary. The efficiency of the linear reweighting focusing inversion method is applied for two sets of gravity horizontal gradient data, with and without noise, related to two synthetic models. The subsurface density contrasts distribution obtained from the analysis of the synthetic models by this inversion method has well determined the underground location of the farther edges of the anomaly source. This method is used to detect the underground edges of a chromite mass in Sabzevar. Also, to compare and validate the results, three conventional local phase filters namely the analytical signal, tilt angle, and total horizontal differential have been used to detect the anomaly source border. The results obtained from various methods show an acceptable conformity in chromite mass border detection. Based on the analysis conducted over real gravity data, the depth of the farthest subsurface vertical borders is between a range of 5 to 10 meters, and the highest horizontal expansion was around 26 meters.

Key words: Chromite, gravity horizontal gradient, linear reweighting focusing inversion.

Resumen

Existen numerosos métodos para detectar el borde de la fuente de anomalías de campos gravimétricos y magnéticos, la mayoría de los cuales se basan en la combinación de gradientes horizontales y verticales de primer y segundo orden del campo potencial. Los métodos de detección de bordes basados en gradientes y otros métodos determinan los límites de la fuente de anomalías en la superficie del suelo. En el presente estudio, se utilizó un método de inversión de enfoque de reponderación lineal para detectar los bordes verticales de una masa subterránea. La ventaja de este método sobre los métodos convencionales es que mediante el uso de datos de gradiente horizontal de gravedad en el método de inversión de enfoque de reponderación, podemos detectar las fuentes de anomalías del subsuelo. La eficiencia del método de inversión de enfoque de reponderación lineal para dos conjuntos de datos de gradiente horizontal de gravedad se evaluó en dos modelos sintéticos (ruidoso y silencioso). La distribución de densidad del subsuelo obtenida del análisis de los modelos sintéticos mediante este método de inversión estimó bien la ubicación subterránea de los bordes más lejanos de la fuente de la anomalía. Este método se utiliza para detectar los bordes subterráneos de una masa de cromita en Sabzevar. Además, para comparar y validar los resultados, se utilizaron tres filtros de fase locales convencionales, a saber, la señal analítica, el ángulo de inclinación y el diferencial horizontal total, para detectar el borde de la fuente de anomalía. Los resultados obtenidos de varios métodos muestran una conformidad aceptable en la detección de bordes de masa de cromita. Según el análisis realizado, la profundidad de los bordes verticales del subsuelo más lejanos osciló entre 5 y 10 metros, y la expansión horizontal más alta fue de alrededor de 26 metros.

Palabras clave: cromita, gradiente horizontal de gravedad, inversión de enfoque de reponderación lineal.

Received: March 19, 2024; Accepted: November 17, 2024; Published on-line: April 1, 2025.

Editorial responsibility: Dr. Joel Rosales-Rodríguez

* Corresponding author: Mahsa Kabiri, mahsa_kabiri@yahoo.com

¹ Islamic Azad University, Faculty of Geological Science and Civil Engineering, Department of Geophysics, Central Tehran Branch, Tehran, Iran.

² Islamic Azad University, Faculty of Basic Science, Department of Geology, Chaluos Branch, Chaluos, Iran.

Mahsa Kabiri, Zohreh Sadat Riazi Rad

<https://doi.org/10.22201/igeof.2954436xe.2025.64.2.1790>

1. Introduction

The ground gravity field maps are widely used for mineral resources exploration programs. The obtained images consist of anomalies with various intensities and wavelengths which are covered by the noises with various amplitudes in most cases. Therefore, to extract the details on the map and highlight the structures and shape of gravity anomaly sources with various intensities, the filtering technique has been used. There are various filters to enhance and estimate the causative body edges of the potential field. Regarding the nature of the data and the domain of changes in the intensity of anomalies existing in the images as well as the filtering objective, various types of filters have been used.

Today, one of the filters widely used for the interpretation of gravity field data is the local phase filter. The most important advantage of such filters is their flexibility, in a way that, with a slight change in the formula of a filter, and in fact, their normalization, new and yet more efficient filters can be produced. Local phase filters are obtained by combining the horizontal and vertical derivative of gravity data with different orders. such as the analytical signal method (Nabighian, 1972 & 1974), the tilt angle filter (Miller and Singh, 1994), the total horizontal derivative (Verduzco *et al.*, 2004), theta map (Wijns *et al.*, 2005), the directional tilt angle and the real part of the hyperbolic tangent function (Cooper, 2006), balanced profile curvature filter (Cooper, 2009), generalized derivative operator (Cooper and Cowan, 2011), normalized total horizontal derivative filters (Cooper, 2006; Ma and Li, 2012), and angle of deviation of the total horizontal gradient filter (Ferreira *et al.*, 2011 & 2013).

Yuang *et al.* (2014) suggested three optimized methods to balance the large eigenvalues of the data in a way that these eigenvalues are located on the edge of the anomaly source. Eshaghzadeh and Kalanitari (2017) offered the use of the Canny edge detection algorithm for the analysis of the potential fields. Görgün and Albora (2017) used the directive filter method to analyze the gravity field. Eshaghzadeh *et al.* (2018) use the balanced generalized horizontal derivative tilt angle filter to analyze the potential field data. Also, the wavelet analysis method has been used to detect the border of the mass of gravity anomaly source (Alp *et al.*, 2011; Eshaghzadeh *et al.*, 2019).

All the mentioned methods detect the subsurface causative mass border on the map and practically they give no idea of how deep the edges of underground structure are. Thus, it is needed to, besides this edge detection method, also use another qualitative-quantitative method so that a correct interpretation of the area under evaluation and expansion of the subsurface source can be provided. To do so, we have used a 2-D inversion method to detect the vertical borders of underground mass.

Numerous inversion methods have been provided by various researchers such as Kriging (Shamsipour *et al.*, 2012), inversion by gravity gradient tensor (Hou *et al.*, 2015; Zhen-Long *et al.*, 2019), conjugate gradient method (Tai-Han *et al.*, 2017; Tian *et al.*, 2018), the weighted method (Rezaie *et al.*, 2016), Modular Feed-forward Neural Network (Eshaghzadeh and Hajian, 2018), PSO algorithm (Eshaghzadeh and Sahebari, 2020), and damped SVD and Marquardt inverse methods (Eshaghzadeh and Hajian, 2020).

Through the error and trial and the use of various inversion methods, we finally concluded that using a reweighting focusing inversion method of the gravity horizontal gradient data is suitable for the detection of the edge of the subsurface anomaly source mass. The efficiency of this method is evaluated using two subsurface synthetic models, and in the following, real gravity horizontal gradient data due to a Chromite mass will be analyzed.

2. Methodology

In the linear inversion method, the subsurface ground is divided into a network of equal-sized cubes (cells) with a constant density contrast (in two-dimensional mode, the ground is actually divided into equal-sized rectangles along the data collection profile). The density contrast inside each cell is the unknown parameter in the linear inverse problem. Figure 1 shows an example of two-dimensional subsurface ground divided into equal cubes.

We need to calculate the kernel matrix (also known as the Jacobian matrix, the leading operator matrix, the sensitivity matrix, or the model matrix) for the gravity field. The kernel matrix is the calculation of the effects of gravity of each cube in Figure 1 (jth cube) in the point of calculation **i**. Therefore, considering Figure 1, in each point of calculation on the ground surface, N×M of gravity effect is computed.

Various formulas have been provided for the calculation of the gravity effect of the cube (in 3-D case) or rectangle (in 2-D case).

The gravity effects of the rectangular block can be computed by following equation (Gerkense *et al.*, 1989).

$$d_z = G \rho \sum_{i=1}^2 \sum_{j=1}^2 \sum_{k=1}^2 \mu_{ijk} \begin{bmatrix} z_k \arctg \frac{x_i y_j}{z_k R_{ijk}} \\ -x_i \cdot \log(R_{ijk} + y_j) \\ -y_j \log(R_{ijk} + x_i) \end{bmatrix} \quad (1)$$

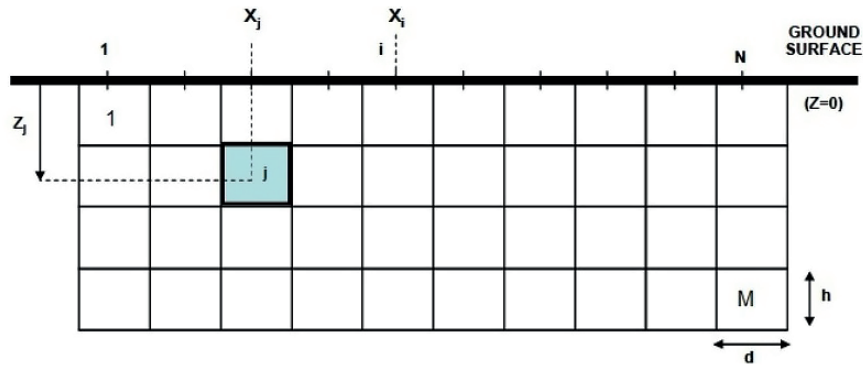


Figure 1. A 2-dimensional Schematic view of subsurface ground division into equal-sized cubes.

Where,

$$R_{ijk} = \sqrt{x_i^2 + y_j^2 + z_k^2}$$

$$\mu_{ijk} = (-1)^i (-1)^j (-1)^k$$

In the last equations, G is the gravitational constant, ρ is density, z is the center depth of each block, and x is the distance from the point of calculation to the origin.

Based on Figure 1, the equation of gravity linear inversion can be written as follows:

$$G_{N \times M} m_M = d_N^{obs} \quad (2)$$

Where G is the Kernel matrix. The Kernel matrix represents the gravity effect of gridded subsurface inversion domain at all points of calculation on the ground surface without applying the density value of each cell (blocks of grid). In the gravity inversion, the objective is to determine the approximate response m (density contrast of each cell) using the known values of G and d^{obs} (data vector). If the observed gravity anomalies are produced by M subsurface cells, the gravity anomaly in the i th point will be estimated as follows:

$$d_i = \sum_{j=1}^M G_{ij} m_j \quad (3)$$

Where $i=1, \dots, N$, d_i is the observed gravity at i th point, m_j is the density contrast of j th cube, and G_{ij} is the effect of j th subsurface cell at i th point.

In the gravity inversion, the Kernel matrix value quickly decreases with increasing depth. Therefore, the reconstructed model is focused near the surface, and it is needed to use a depth weighting function to neutralize the reduction in kernel sensitivity with depth (Li & Oldenburg, 1996; Pilkington, 1997).

2.1 Reweighting Focusing Inversion

The main objective of gravity inversion problems is to find a geologically acceptable density model based on the sensitivity matrix and the data measured at a level of noise. In the present study, we aimed to determine the density distribution that corresponds to the vertical borders of the mass subsurface structure, so our input data will be gravity horizontal gradient instead of gravity data. As mentioned, gravity inversion problems are usually ill-posed and the solutions can be non-unique or unstable. We can solve these problems by the minimization of Tikhonov parametric functional (Tikhonov & Arsenin, 1977):

$$\phi^\mu(m) = \varphi(m) + \mu S(m) \quad (4)$$

Where μ is the regularization parameter, $\varphi(m)$ is the misfit function, and $S(m)$ is the stabilizer function or model objective function. Equation 4 can be written as follows (Rezaie *et al.*, 2016):

$$\phi^\mu(m) = \|W_d(Gm - d)\|^2 + \mu \|m\|^2 \quad (5)$$

W_d is the data weighting matrix which is defined as $W_d = \text{diag}(1/\sigma'_1, \dots, 1/\sigma'_N)$, and σ'_i is the standard deviation of noise in the i th data. In an inversion, the objective function is generally defined as follows (Oldenburg & Li, 2005):

$$\phi(m) = \|Gm - d\|^2 + \mu \|W_m(m - m_{ref})\|^2 \quad (6)$$

Where W_m is the weighting matrix for the model's parameters (model weighting matrix).

To produce compact solutions, we select a stabilizer equal to the minimum support functional as follows (Portniaguine & Zhdanov, 1999):

$$S(m) = \sum_{j=1}^M \frac{m_j^2}{m_j^2 + \beta^2} \quad (7)$$

Where β focusing parameter is a predefined small positive number so that it can prevent the uniqueness of the response when $m_j=0$, and m_j is the j th element of vector m .

By placing the minimum norm stabilizing functional in Equation 5, we will have:

$$\phi(m) = \|Gm - d\|^2 + \mu \sum_{j=1}^M \frac{m_j^2}{m_j^2 + \beta^2} = \min \quad (8)$$

This problem is solved by the reweighting optimization (Mehanee *et al.*, 1998). To calculate the various sensitivities of the data to the model's parameters, a diagonal weight matrix (\hat{W}_m) is considered for the model's parameters (Portniaguine & Zhdanov, 2002). Mehanee *et al.* (1998) and Portniaguine & Zhdanov (1999) indicated that the weight matrix can be computed from the root of the cumulative sensitivity matrix:

$$\hat{W}_m = \sqrt{\hat{S}} \quad (9)$$

Where \hat{S} is the diagonal matrix that is formed by data cumulative sensitivity for the parameter m_j , set as the following equation (Portniaguine & Zhdanov, 2002):

$$S_j = \frac{\|\delta d\|}{\delta m_j} = \sqrt{\sum_i (G_{ij})^2} \quad (10)$$

In Equation 10, G_{ij} is the element of the forward operator matrix (Kernel matrix). The diagonal elements of the matrix \hat{W}_m are determined by $\{\omega_1, \omega_2, \dots, \omega_j, \dots, \omega_{N_m}\}$. Also, the depth weighting matrix can be computed by $W_m = \text{diag}(1/(z_1)^\lambda, \dots, 1/(z_M)^\lambda)$. In this equation, z_j is the depth of the j th parameter of the model, and the optimal value of λ for the reweighting focusing inversion method in the present study is equal to 0.5.

Substituting the weighting matrix in Equation 8, and choosing $m_{ref}=0$, we will have:

$$\phi(m) = \|\hat{G}m - \hat{d}\|^2 + \mu \sum_{j=1}^M \frac{\omega_j^2 m_j^2}{m_j^2 + \beta^2} = \min \quad (11)$$

Where $\hat{G}=W_d G$ and $\hat{d}=W_d d$. The reweighting matrix $\hat{W}(m)$ will be as follows (Portniaguine & Zhdanov, 2002):

$$\hat{W}^2(m) = \text{diag}[m^2 + \beta^2 I] W_m^{-2} \quad (12)$$

Where diag is the diagonal matrix produced by $m^2 + \beta^2$, and I is the singular matrix. Also:

$$m_w = \hat{W}^{-1}(m) m \quad (13)$$

and

$$G_w = \hat{G} \hat{W}(m) \quad (14)$$

Equation 11 is written as follows:

$$\phi(m_w) = \|G_w m_w - \hat{d}\|^2 + \mu \|m_w\|^2 \quad (15)$$

Equation 15 is similar to the classical minimum norm optimization problem whose solutions are based on the regularization theory (Tikhonov *et al.*, 1977). The only prominent difference is the new progressive modeling operator, which is $G_w = \hat{W} \hat{G}(m)$, that depends on the m_w , and changes during the inversion (Portniaguine & Zhdanov, 2002). To obtain acceptable results, the maximum and minimum values are defined for the model's parameter ($[m_{min}, m_{max}]$) (Portniaguine & Zhdanov, 2002; Portniaguine & Zhdanov, 1999).

Both expressions of the objective function (Equation 15) are 2-norm and thus, differentiable. The prevalent method to solve Equation 15 is using the least squares method. Then, Equation 15 is equal to:

$$\phi(m_w) = (G_w m_w - \hat{d})^T (G_w m_w - \hat{d}) + \mu m_w^T m_w \quad (16)$$

$$\phi(m_w) = G_w^T m_w^T G_w m_w - G_w^T m_w^T \hat{d} - \hat{d}^T G_w m_w + \hat{d}^T \hat{d} + \mu m_w^T m_w \quad (17)$$

Regarding the dominant relationships about gradient calculation, that is:

$$\begin{aligned} \nabla_x X^T Y &= Y \\ \nabla_x X Y^T &= Y \\ \nabla_x \left(\frac{1}{2}\right) X^T Y X &= Y X \end{aligned} \quad (18)$$

By computing the derivative of Equation 17 with respect to the model parameter m_w , and setting the derivative equal to zero, we will have:

$$\frac{\partial \phi(m_w)}{\partial m_w} = 2G_w^T G_w m_w - G_w^T \hat{d} - \hat{d} G_w^T + 2\mu m_w \quad (19)$$

$$2m_w (G_w^T G_w + \mu) = 2G_w^T \hat{d} \quad (20)$$

As a result, we will have:

$$m_w = (G_w^T G_w + \mu)^{-1} (G_w^T \hat{d}) \quad (21)$$

m_w is computed using Equation 21. m_w and $\hat{W}(m)$ are updated in each iteration until m satisfies the iteration convergence criterion (predetermined acceptable error).

The value of μ of the regularizing parameter is computed for each iteration as follows:

$$\mu = \frac{\|G_w m_w - \hat{d}\|^2}{\|m_w\|^2} \quad (22)$$

During the inversion, for each iteration, 2-norm error between the observed and computed gravity horizontal gradient data are estimated:

$$Q_k(d) = \sqrt{\sum_{i=1}^N (d_i^{cal} - d_i^{obs})^2} \quad (23)$$

Where, d^{cal} is the computed gravity horizontal gradient corresponding to parameters of the estimated model (subsurface density distribution) in each iteration, and d^{obs} is the observed or measured gravity horizontal gradient field. The stopping criteria of the inversion process are defined as follows:

1. The 2-norm values of observed and computed gravity horizontal gradient difference in each iteration be less than the predetermined value, i.e., $Q_k \leq Q_{initial}$.
2. The 2-norm values of observed and computed gravity horizontal gradient difference in one iteration be higher than the previous iteration, i.e., $Q_k \geq Q_{k-1}$.

3. The number of considered iterations for the inversion process be completed.

The modeling algorithm by the reweighting focusing inversion method is represented in Table 1.

3. Analysis of Gravity Horizontal Gradient Data for Synthetic Models

In this section, two synthetic models are considered, and the computed gravity horizontal gradient data for these models will be analyzed using the reweighting focusing inversion method:

3.1 Synthetic Model No. 1

Figure 2(a) represents the measured gravity field in 15 points on a gridded underground which has been divided into 150 cells as 9 of them have a density contrast of 1000 Kg/m³ (Figure 2b). The area with density difference is located at a depth of 15 to 30 meters, with a length of 60 meters along the profile (120 to 180 meters far from the starting point). The distance between the data sampling points (length of each cell) is 20 meters and the length of the profile is 280 meters.

The value of the considered initial error between the computed gravity gradient and the inverted gravity gradient, as one of the stopping criteria for iterations in the inversion process, is equal to 0.004 mGal/m, and $\beta = 0.001$. Also, we set the number of iterations for the inversion process as 30 repetitions.

The changes in the gravity horizontal gradient field of the synthetic model has been shown by the red curve in Figure 3(a). The subsurface density distributions resulted of the inversion with a different sign have been taken place on the vertical borders of

Table 1. Reweighting focusing Inversion algorithm

Inputs: G $Q_{initial}$, m_{max} , m_{min} , W_d , β , d , m_{prior}
Stage 1: place $k=1$, $m^{(0)} = m_{prior}$, calculate W_m
Stage 2: calculate $\hat{d} = W_d d$, $\hat{G} = W_d G$
Stage 3: Calculate $\hat{W}(m)^{(k)}$, $G_w^{(k)} = \hat{G} \hat{W}(m)^{(k)}$, $m_w^{(k)} = \hat{W}^{-1}(m)^{(k)} m^{(k-1)}$, $\mu^{(k)}$
Stage 4: Calculate $m_w^{(k)} = (G_w^T G_w + \mu)^{-1} (G_w^T \hat{d})$
Stage 5: Calculate $m^{(k)} = \hat{W}(m)^{(k)} m_w^{(k)}$
Step 6: Apply density limits in a way that: $m_{min} \leq m^{(k)} \leq m_{max}$
Stage 7: Place $k=k+1$
Step 8: Check the stop criteria, if satisfied, stop the process, otherwise, go to step 3.
Output: $m^{(k)}$

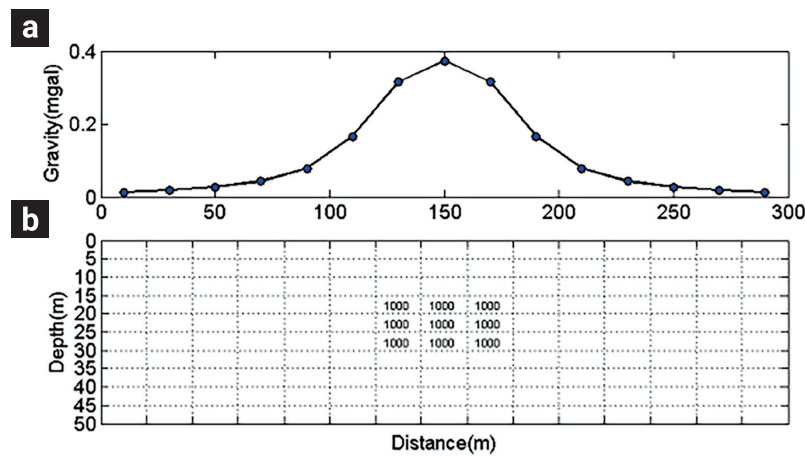


Figure 2. a) Alternations curve of the gravity field due to b) supposed subsurface model with a density distribution of 1000 kg/m³.

the anomaly source (Figure 3(b)). The gravity horizontal gradient field obtained from the inversion is depicted in Figure 3(a) by the circle symbols and blue dashed lines.

As seen in Figure 3(b), the maximum and minimum values of gravity horizontal gradient are located on the vertical borders of the anomaly source mass, and the positive and negative density distributions corresponding to these values have clearly detected the depth of vertical borders. The gravity gradient is commonly used for edge detection. Although these density distributions could not estimate the depth expansion of the border clearly, they are able to detect the depth of the top surface of the anomaly body.

As seen in Figure 4, the 2-norm error value between the computed gravity gradient and the gravity horizontal gradient data obtained from the inversion reduces drastically in the 11th iteration and reaches to 0.0036 mGal/m in the 12th iteration. This value is lower than the initial assumed error value and as a result, the inversion process was stopped.

To examine the efficiency of the reweighting focusing inversion method with noise, 20% random noise is added to the theoretical gravity horizontal gradient field in Figure 2(a), based on the following equation:

$$d_{rand}(x_i) = d(x_i)[1 + (RAN_{(i)} - 0.5) \times 0.2] \quad (24)$$

The value of the considered initial error between the computed gravity horizontal gradient and the inverted ones, as one of the stopping criteria for iteration in the inversion process, is equal to 0.005 mGal/m, and $\beta=0.001$. Also, 40 repetitions have been considered as iteration number during inversion process. The noise contaminated gravity horizontal gradient field due to the synthetic model are depicted by the red curve in Figure 5(a). The recovered subsurface density distributions from the inversion with a different sign have been lied on the vertical borders of the

anomaly source (Figure 5(b)). The inverted gravity horizontal gradient field is illustrated in Figure 5(a) by the circle symbols and blue dashed lines.

As seen in Figure 5(b), the maximum and minimum values of gravity horizontal gradient are located on the vertical borders of the anomaly source mass, and the positive and negative density distributions corresponding to these values have partially detected the depth of vertical borders.

As seen in the last figure, due to the presence of the noise, several small density distributions with low amplitude have been also detected after inversion. Also, the positive density distribution has detected the depth expansion of the source vertical border better than the negative density distribution. As shown in Figure 6, the value of 2-norm error between the computed gravity horizontal gradient and inverted gravity horizontal gradient data shows a sharp decrease in the 16th iteration and reaches 0.0049 mGal/m, which is lower than the initial assumed error value, and as a result, the inversion was stopped in the 16th iteration.

3.2 Synthetic Model No.2

Figure 7(a) represents the estimated gravity field in 20 points on a gridded subsurface that is discretized into 20×10=200 rectangular prisms with a size of 20 meters in x direction and 5 meters in z direction, as 16 of them have a density of 2000 Kg/m³ (Figure 7(b)). The area with a density contrast of 2000 Kg/m³ is located at a depth of 15 to 35 meters, with a length of 100 meters along the profile (140 to 240 meters from the starting point). The distance between the data sampling points (length of each cell or block) is 20 meters, therefore the length of the profile is 380 meters.

The value of the defined initial error between the computed gravity horizontal gradient and the inverted ones, as one of the

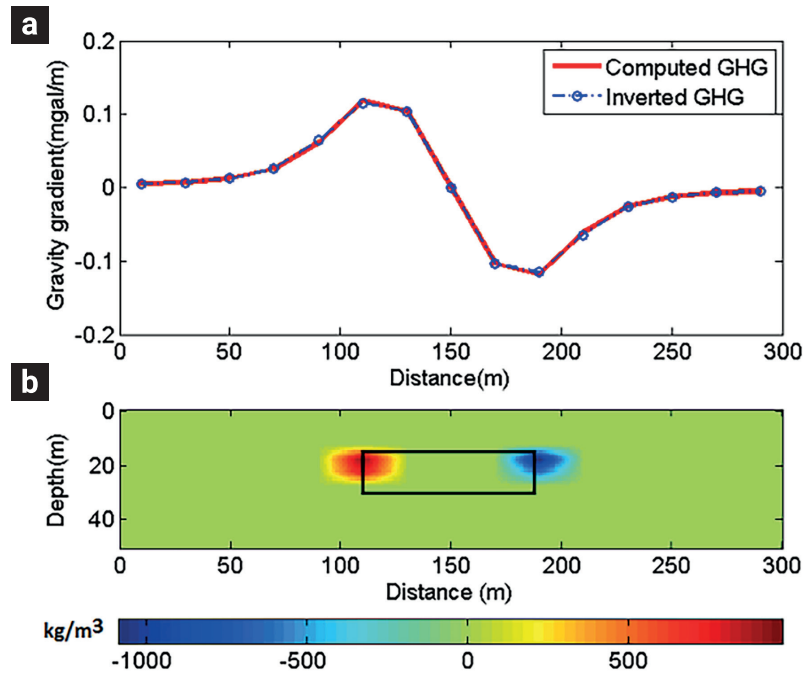


Figure 3. a) the computed gravity horizontal gradient and the horizontal gradient data obtained from the inversion according to b) Subsurface density distribution obtained from the inversion for the synthetic model No.1

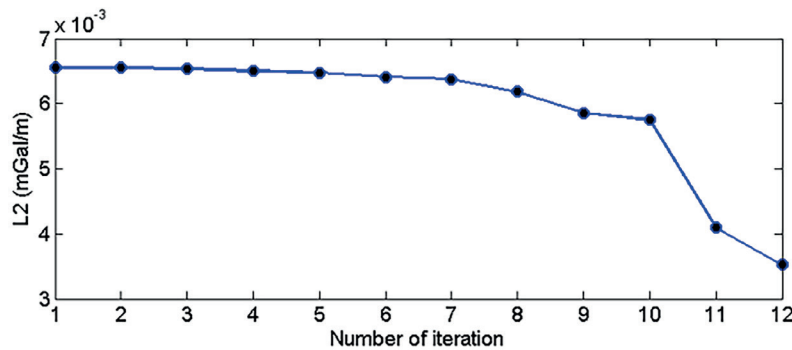


Figure 4. changes in the 2-norm errors between the computed gravity horizontal gradient and obtained ones from the inversion in each iteration for the synthetic model No.1.

stopping criteria for iteration in the inversion process, is equal to 0.04 mGal/m, and $\beta = 0.01$. Also, 50 repetitions have been considered as iteration number during inversion process.

The changes in the gravity horizontal gradient field of the synthetic model No.2 is shown by the red curve in Figure 8(a). Since the vertical border of the anomaly source is stepped, as seen in Figure 8(b), the maximum and minimum values of gravity horizontal gradient have almost conformity to the middle of the stepped border of the anomaly source mass. Nonetheless, the subsurface density distributions resulted from the inversion, where they have the different sign, have been located on the

farther vertical borders of the anomaly causative mass and have been approximately detected their depth expansions (Figure 8(b)). Therefore, using the maximum and minimum values of gravity gradient as an edge detector of the anomaly source can include errors. The inverted gravity horizontal gradient data is shown in Figure 8(a) by the circle symbols and blue dashed lines.

As shown in Figure 9, the value of error between the computed gravity horizontal gradient and the inverted ones is 0.0357 mGal/m in the 17th iteration, which is lower than the initial assumed error value, and as a result, the inversion was stopped in this iteration.

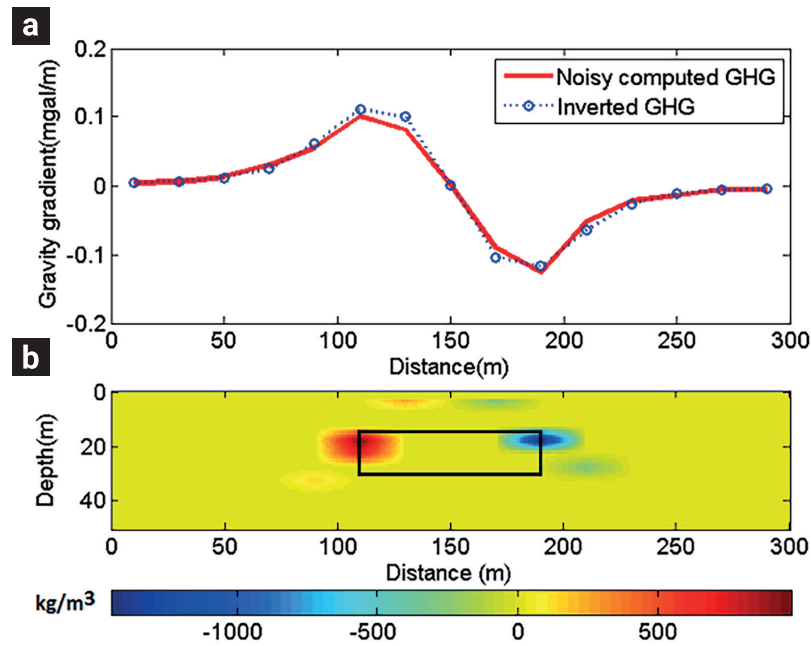


Figure 5. Noise corrupted synthetic gravity horizontal gradient and inverted gravity horizontal gradient due to b) recovered subsurface density distribution for the model No.1.

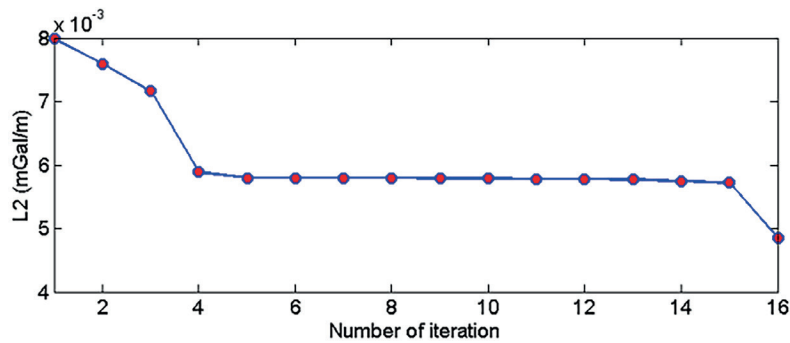


Figure 6. Changes in the 2-norm error between computed noisy gravity horizontal gradient and inverted ones in each iteration for the synthetic model No.

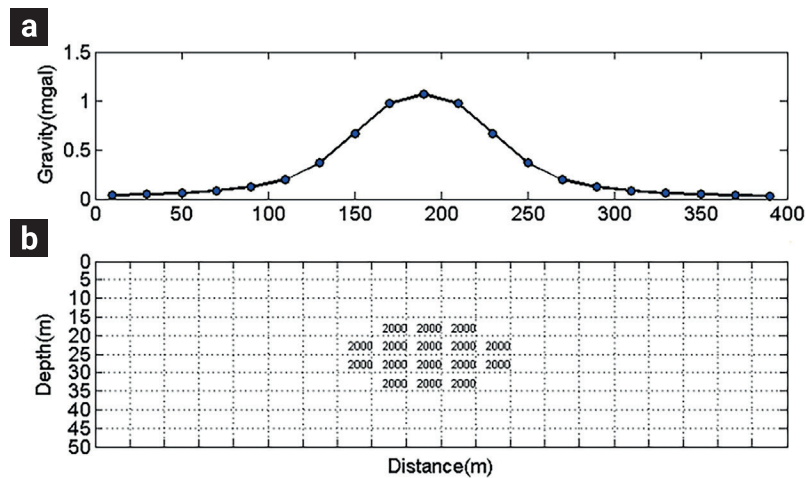


Figure 7. a) Alternations curve of the gravity field due to b) supposed subsurface model with a density distribution of 2000 kg/m³ (synthetic subsurface model No.2).

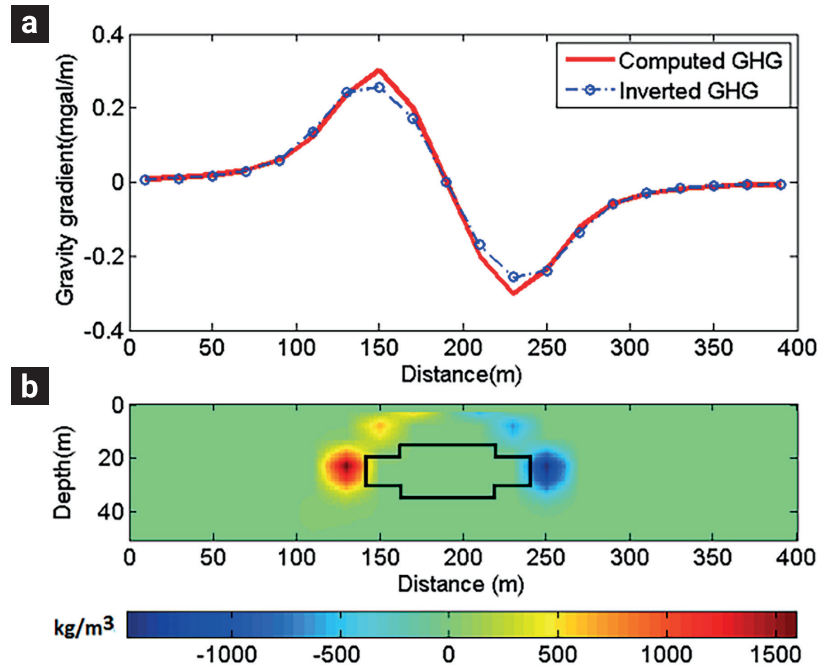


Figure 8. a) computed gravity horizontal gradient and the inverted gravity horizontal gradient due to b) recovered subsurface density distribution for model No.2

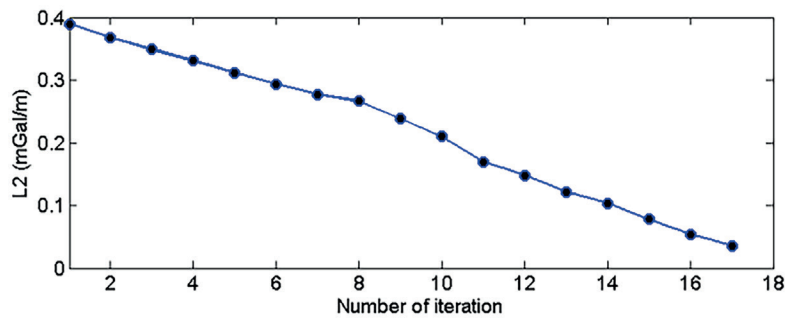


Figure 9. Alterations in the 2-norm errors between estimated gravity horizontal gradient and inverted gravity horizontal gradient in each iteration for the synthetic model No.2.

We have studied the proficiency of the reweighting focusing inversion method by adding 20% random noise to the theoretical gravity horizontal gradient data in Figure 7(a), based on Equation 24.

Figure 10(a) shows the gravity horizontal gradient field of the synthetic model No.2 by the red curve as is noise corrupted. The predefined error value was set as 0.06 mGal/m and $\beta=0.01$. Also, 50 repetitions were assumed for the iteration number during the inversion process. The obtained results of the inversion, that is subsurface density distribution with a different sign are placed on the vertical borders of the anomaly source (Figure 10(b)). The inverted gravity horizontal gradient field corresponding to

the underground density distribution has been depicted in Figure 10(a) by the circle symbols and blue dashed lines. The interpretation of inversion results due to noise corrupted gravity horizontal gradient data is similar to the generated ones without noise.

As seen in the figure 10(b), due to the presence of the noise, several small density distributions with low amplitude in the underground sub-space have been detected.

As shown in Figure 11, the value of 2-norm error between the computed gravity gradient and the inverted horizontal gradient is 0.0506 mGal/m in the 18th iteration, which is lower than the initial assumed error value, and as a result, the inversion was stopped in this iteration.

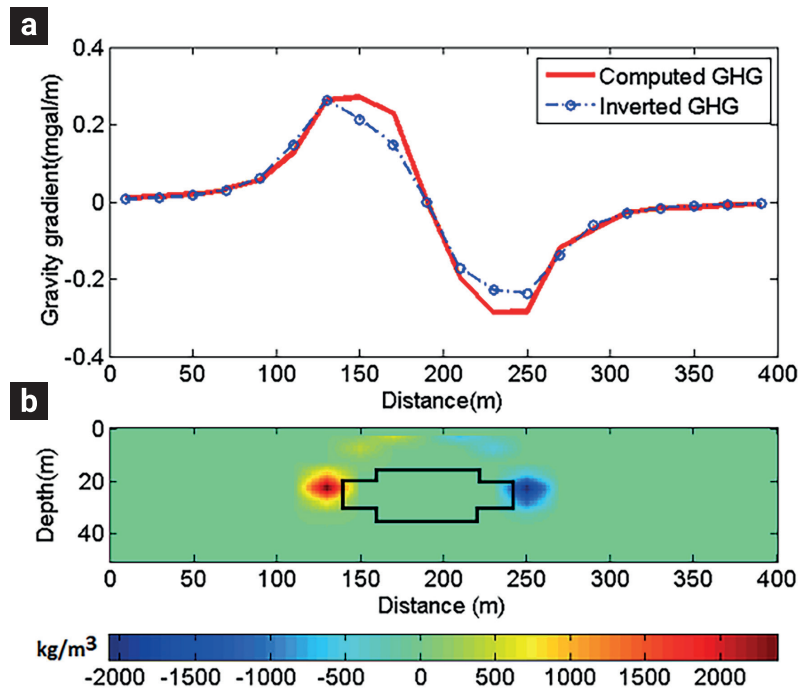


Figure 10. Noise corrupted synthetic gravity horizontal gradient and inverted gravity horizontal gradient due to b) recovered subsurface density distribution for model No.2.

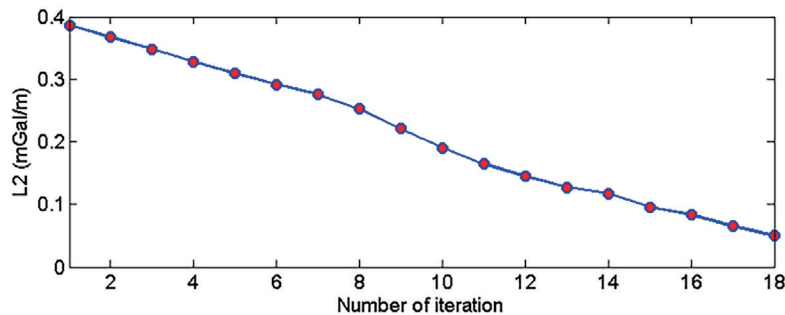


Figure 11. Alterations in the 2-norm errors between estimated noisy gravity horizontal gradient and inverted gravity horizontal gradient in each iteration for the synthetic model No.2.

4. Sabzevar Chromite

In this chapter, we will get familiar with the location and geological structure of the area under investigation in Sabzevar, and then, we will analyze the gravity horizontal gradient data due to a subsurface Chromite mass.

4.1 Location and Geology of the Studied Zone

The study area is located in the North 40th zone of UTM coordinates between the longitudes of 607000 to 607120 meters in

the west-east direction and the latitudes of 4012200 and 4012300 meters in the south-north direction, between the cities of Sabzevar and Neishabur, which includes an area of about 12000m². This area is located in the Sabzevar within the large structural zone of Central Iran. In a broader view, this area is located between two major faults and infrastructures, Darouneh (in the south) and Binaloud fault (in the north). The Sabzevar zone is connected to the Binalood zone from the north and the Loot block zone from the south. These connections are tectonic and faulted.

In fact, the Sabzevar region is a part of the Ophiolitic region that extends from the east to the south of the country. The struc-

tural form of the study area is undoubtedly influenced by faults such as Darouneh and Taknar. The construction direction of this area follows the Darouneh fault direction.

The Sabzevar area contains a large number of chromite masses in the form of strings and large and small lenses. The igneous masses of this area are stretched in an almost east-west direction and are primarily composed of alkaline rocks. Chromite masses are spread irregularly but with a certain concentration in these rocks. The amount of their alloy is very variable. Burrows *et al.* (1983) attribute the age of the Ophiolitic complexes to the Upper Cretaceous (Koniasian).

In the study area, the limited rock outcrops include ultrabasic igneous rocks that are mostly transformed into serpentine and minerals such as talc and vermiculite (Aghajani, 2012). Figure 12 shows the geological map of the area under study.

4.2 Gravity Field of the Study Area

Figure 13 shows the Bouguer gravity field of the study area in Sabzevar. As can be seen in figure 13, the gravity field has been measured along 6 profiles in the north-south direction and at 56 stations with an approximate distance of ten meters (black circles in Figure 13). Bouguer gravity field include the regional and local anomalies and by processing the Bouguer gravity field data can detect the positive and negative local anomalies.

Therefore, it is necessary to remove the regional field from the Bouguer gravity field using the 2-degree surface trend method so that the residual gravity anomaly will be obtained. Almost, all the qualitative and quantitative analyses are performed on the residual gravity field.

Figure 14 shows the produced residual gravity field using the second-degree surface trend. Due to the high density difference between the Chromite host rock and the surrounding rocks, we expect chromite-bearing zones to be highlighted on the residual gravity anomaly map with a positive gravity value. As seen in the residual gravity anomaly map in Figure 14, a region with the maximum positive gravity field value has been detected in the southern part, which most likely has a source body that forms the chromite host rock.

For 2-D modeling of the subsurface causative mass, we analyze the residual gravity field variations along the profile AA' which runs across the Chromite mineral mass in an approximately W-E direction as is shown in figure 14. Data sampling has done in 11 points with an interval of 4 m over the profile AA' with a length of 40 m.

4.3 Analysis of Gravity Horizontal Gradient

To analyze the real gravity horizontal gradient along the profile AA' (green curve in Figure 16(a)) using the reweighting focusing

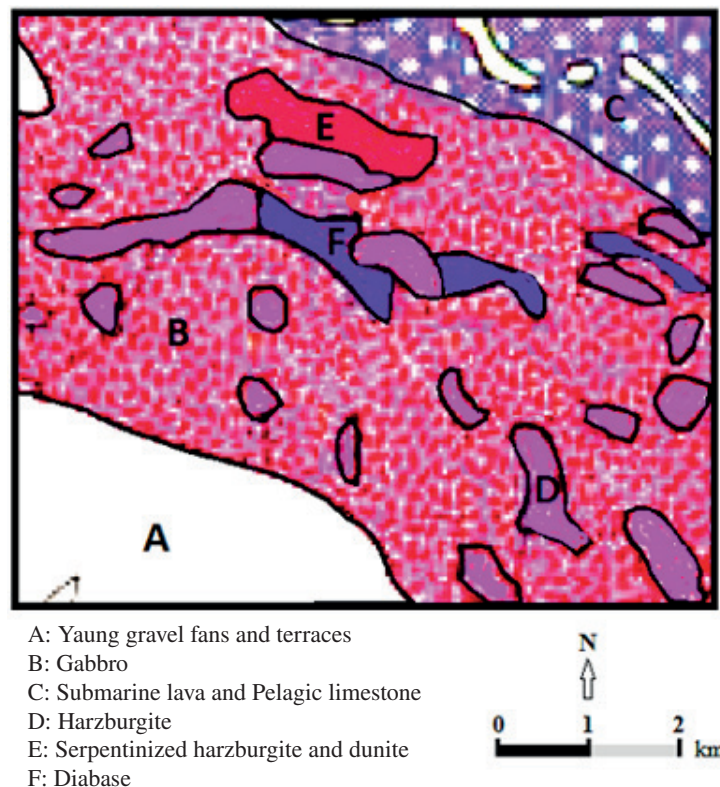


Figure 12. The geological map of the study area in Sabzevar zone.

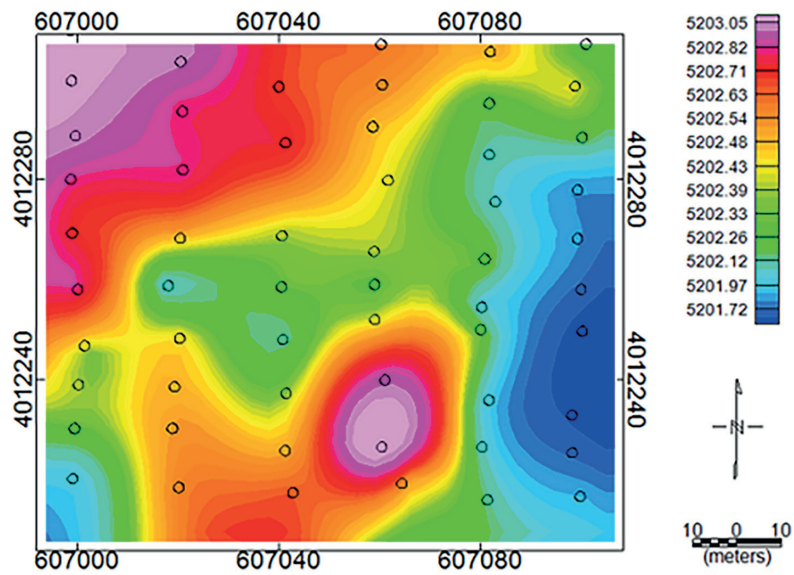


Figure 13. Bouguer gravity field map of the area under investigation as the gravity reading stations have been shown on it by the black circles.

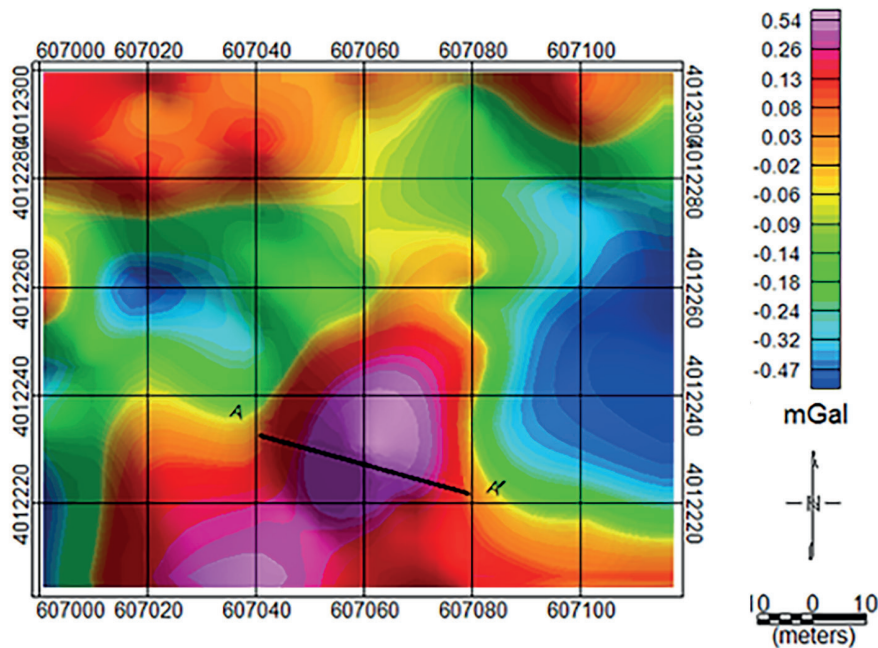


Figure 14. The residual gravity map of the area under investigation. The location and direction of the profile AA' has been shown on the positive gravity anomaly.

inversion, the number of iterations and the value of 2-norm errors between the observed gravity horizontal gradient and inverted ones were set to 25 repetitions and 0.0001 mGal/m, respectively.

Figure 15 shows the changes of 2-norm errors with the increase in the number of iterations. The 2-norm values reached 0.00015 in the 12th iteration and obtained 0.000074 in the 13th iteration, which is lower than the initial assumed error value.

Therefore, the optimized inverted response belongs to the computed density distribution in the 13th iteration. The variations of the gravity horizontal gradient corresponding to the recovered density contrast distributions of the inversion is shown in figure 16(b) as is depicted with the blue dashed curve in Figure 16(a).

As seen in Figure 16(a), a mass with negative values has been located at a depth about 5 meters, 33 meters from the first

data sampling point, and another one with positive values has been settled at a depth between 5 to 10 meters, approximately 7 meters far from the starting point. Based on the obtained results, the maximum horizontal expansion of the anomaly source is around 26 meters.

5. Detection of the Gravity Anomaly Border Using the Conventional Methods

In this chapter, three common edge detector filters namely analytic signal, tilt angle, and total horizontal derivative were used to detect the anomaly source edges as we can compare these results with the estimated border from the reweighting focusing inversion method. Because these filters are applied on the gridding of the gravity field, we can determine the horizontal expansion of the subsurface source through analysis of the obtained maps from these edge detection filters.

5.1 Analytic Signal

Nabighian developed an automated method for the interpretation of 2-D magnetic anomalies based on the analytic signal in some articles from 1972 to 1974. The maximum value of the analytic signal take place on the anomaly causative mass. Using this property of the analytic signal, the location of the source and its edges can be detected. The analytic signal function for the gravity data (T) is defined as:

$$|A(x)| = \sqrt{\left(\frac{\partial T}{\partial x}\right)^2 + \left(\frac{\partial T}{\partial y}\right)^2 + \left(\frac{\partial T}{\partial z}\right)^2} \quad (25)$$

Figure 17 shows the analytic signal map for the study area. As was mentioned, the maximum values of the analytical signal are located on the anomaly source. We have considered values

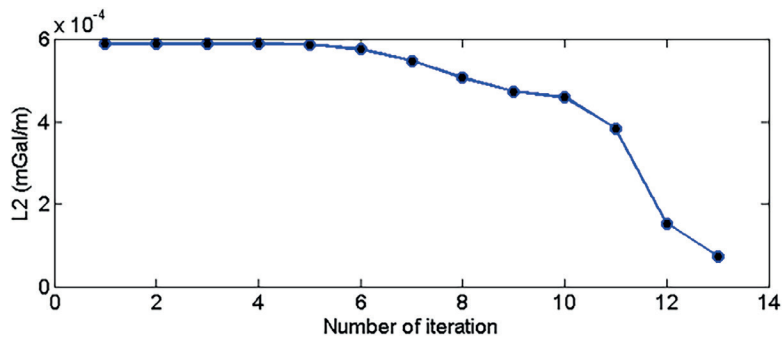


Figure 15. 2-norm error changes in each iteration during real gravity gradient data inversion

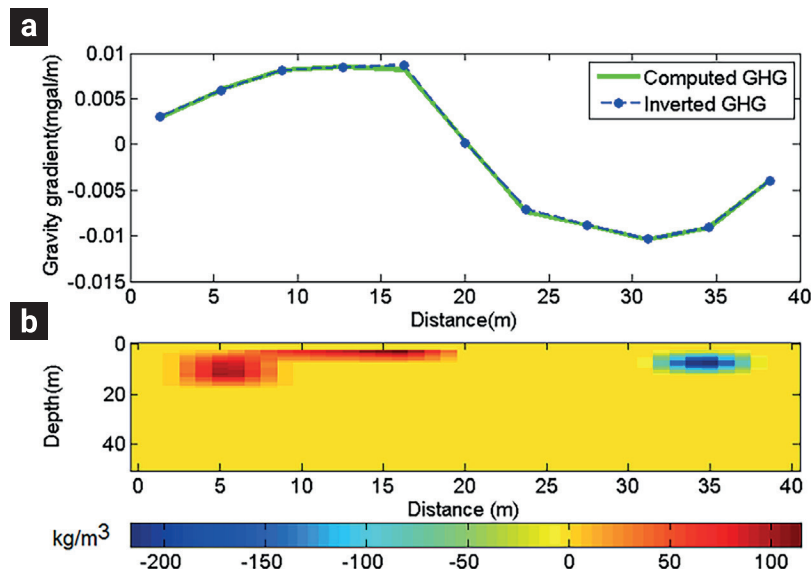


Figure 16. a) Variations of the observed and produced gravity horizontal gradient fields, b) Distribution of density obtained from the reweighting focusing inversion of gravity horizontal gradient along profile AA'.

greater than 0.05 mGal/m as the maximum values of the analytical signal filter. As depicted in Figure 17, a contour line of 0.05 mGal/m has been drawn around the anomaly related to the chromite mass, which is assumed to be the border of the subsurface source. The dashed line shown in Figure 17 almost corresponds to the direction of profile AA'. The length of this dashed line is approximately 25 meters. Therefore, the distance between the edges of the anomaly source along this dashed line is about 25 meters, which closely matches with the distance of the edges which estimated by the inversion method (26 meters).

5.2 Tilt Angle

A prevalent local phase filter is the tilt angle (deviation angle) (Miller and Singh, 1994) which can be easily computed for both frequency and the space domains, and is defined as follows:

$$T = \tan^{-1} \left(\frac{\partial f / \partial z}{\sqrt{\left(\frac{\partial f}{\partial x}\right)^2 + \left(\frac{\partial f}{\partial y}\right)^2}} \right) \quad (26)$$

Where f is gravity or magnetic field. The tilt angle gradient has interesting properties. As a dimensionless ratio, it responds very well to deep and shallow sources and has a wide range of variations for sources at the same level. For a source with positive density, the tilt angle is above the positive anomaly. Near the edges, where the vertical derivative is zero and the horizontal derivative is the largest, the value of the tilt angle is zero, and outside the subsurface anomaly zone, it is negative.

Figure 18 shows the tilt angle of the study area in Sabzevar. The contour line with the zero radian indicates the border of the subsurface sources, as has been drawn on the tilt angle map in figure 18. As observed in Figure 18, the tilt angle filter could not separate a confined part as the border around the gravity anomaly related to the chromite mass. However, since the zero values of tilt angle detect the anomaly source edge, we have connected these values in the east-west direction on the anomaly by a dashed line (Figure 18). This line is 30 meters long which indicates that the horizontal expansion of the subsurface anomaly source in the east-west direction is 30 meters. Although the direction of the dashed line in Figure 18 is not in the same direction as profile AA', the value of the area for the subsurface mass obtained by the tilt angle is acceptably close to the value obtained by the reweighting focusing inversion method.

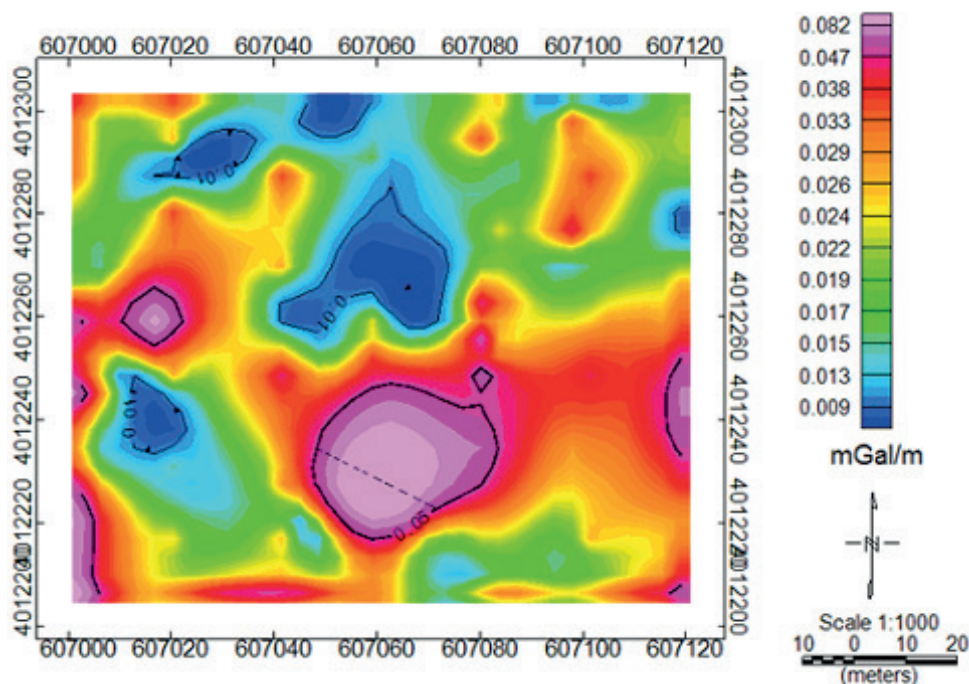


Figure 17. Analytic signal map area under study. The dashed line is almost corresponding to the direction of profile AA' shown in figure 14.

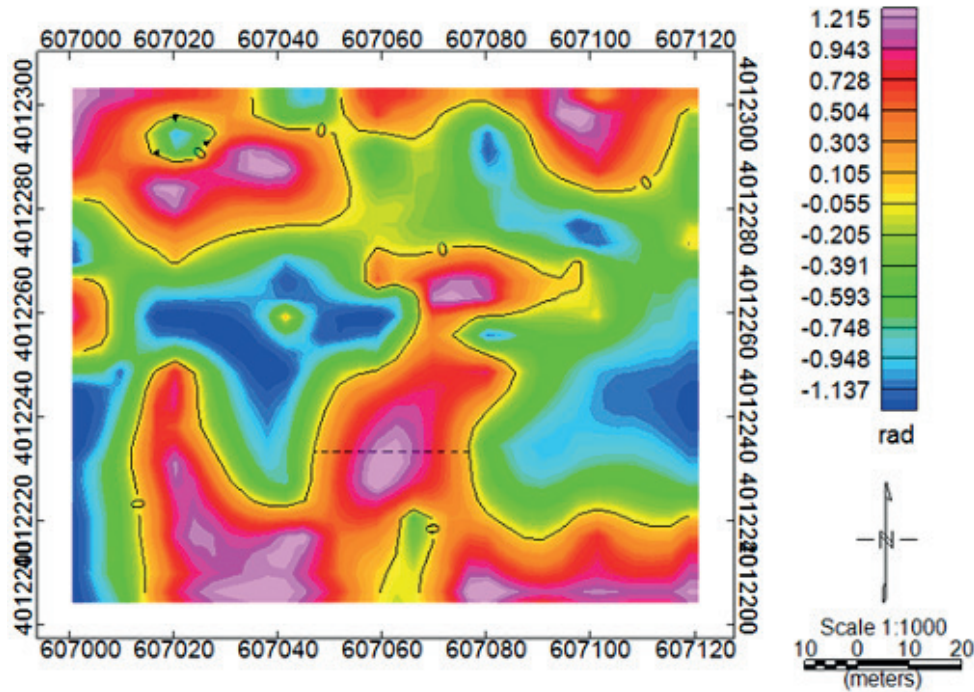


Figure 18. tilt angle map obtained from the gravity data analysis for the study area in Sabzevar.

5.3 Total Horizontal Derivative:

The maximum value of horizontal derivatives, which is also known as the total horizontal derivative which leads to better detection of anomaly edges in any direction, is defined as follows (Cooper, 2006):

$$f_{x_{tot}} = \sqrt{\left(\left(\frac{\partial f}{\partial x}\right)^2 + \left(\frac{\partial f}{\partial y}\right)^2\right)} \quad (27)$$

Figure 19 shows the map obtained from the total horizontal derivative executed on the gravity data related to the study area in Sabzevar. Similar to the tilt angle, this filter also has failed to create a closed curve of its maximum values around the positive anomaly of the chromite mass as the source edge, and it could not detect a specific border. The curve with the same contour of 0.1 mGal/m is shown on the total horizontal derivative map. The maximum values of this filter are located in the middle of this level curve. Similar to Figure 18, a dashed line in the east-west direction connects the maximum values between the 0.1 mGal/m contour lines that correspond to the mass border. This line, which indicates the distance between the eastern and western borders of the mass, is around 34 meters long. Therefore, this filter has estimated the horizontal outspread of causative mass

8 meters higher than the value obtained from the reweighting focusing inversion method.

6. Estimation of Chromite Mass Depth

In this chapter, two common depth estimation methods, namely the Euler Deconvolution and power spectrum (energy density spectrum) methods are used to estimate the depth of the chromite mass. Figure 20 shows the estimated depth by the Euler deconvolution method for a 5×5 window length on the residual gravity field. As seen in this figure, the depth of the top surface of the chromite mass is between 5 to 10 meters.

The power spectrum method estimates the average depth of the top surface of the anomaly source mass about 11.5 meters (the intersection of the horizontal blue line with the depth axis in Figure 21). It should be noted that the power spectrum method uses all the existing wavelengths for estimation of the depth of the top surface of the source masses in the study area, so the overestimation of the depth of the top surface is expected.

7. Non-linear Inverse Modelling

To obtain the shape of the subsurface chromite mass, we

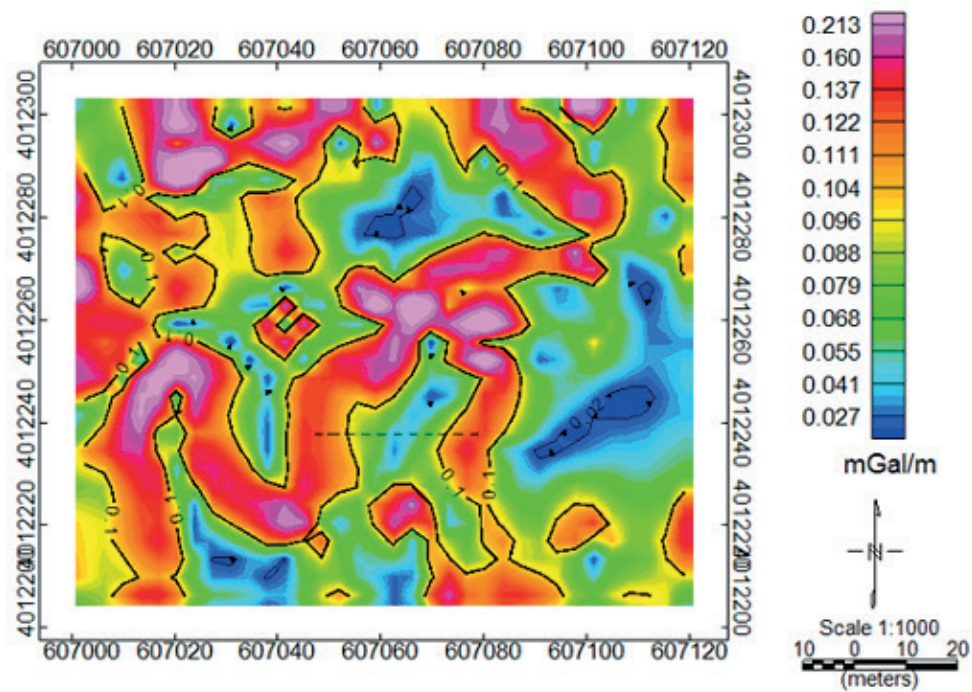


Figure 19. Total horizontal derivative map obtained from the gravity data analysis for the study area in Sabzevar.

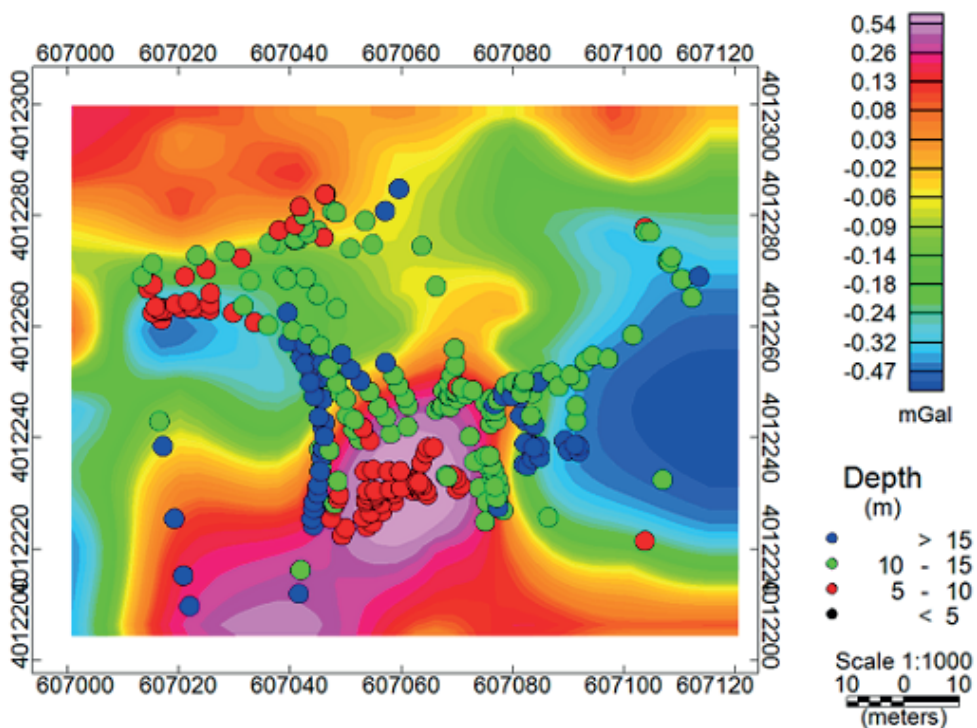


Figure 20. Resulted depth by the Euler Deconvolution method drawn on the residual gravity field map.

used Model Vision software for a two-dimensional non-linear inversion of the gravity field along a profile with a 100 m long, which was almost in the same direction with the profile AA'. Data sampling was done at 11 points at a distance of 10 meters in the direction of the gravity profile. The black curve in Figure 22 shows the gravity field changes along this profile. The structure obtained from the nonlinear inversion for the underground mass is shown in Figure 22. The blue curve in Figure 22 shows the inverted gravity field corresponding to the subsurface mass. Also, the obtained 2-norm error between observed and computed gravity values is 0.41 mGal/m.

Based on Figure 22, the depth of the top surface of the mass is around 5 meters and the highest value of the horizontal expansion

is 21 meters. The eastern border of the mass is shown as a point at a depth of 5 meters, and the western border is a vertical line, almost 7 meters long (5 to 12 meters deep).

8. Conclusion

Analysis of the synthetic models indicates that the use of gravity horizontal gradient data in the reweighting focusing inversion algorithm produces distributions of positive and negative density which correspond to the farthest vertical borders of subsurface mass, and can relatively estimate the deep expansion of the mass. The efficiency of the suggested method in the

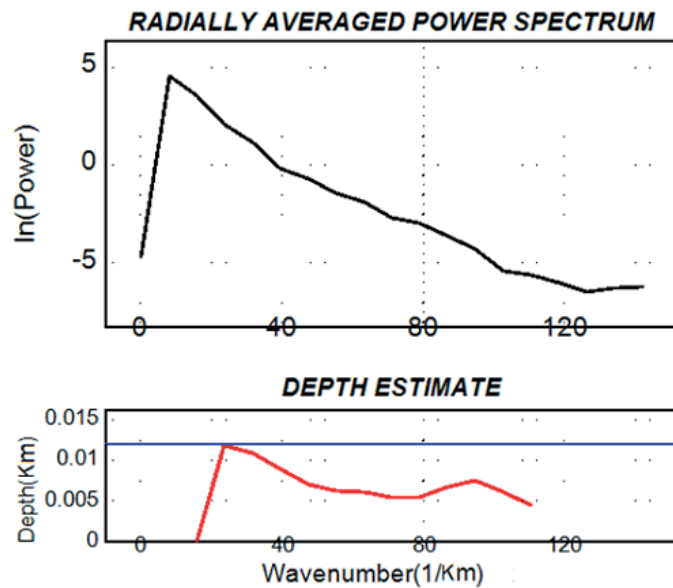


Figure 21. Analysis of the average depth of the top surface of chromite mass using the power spectrum method.

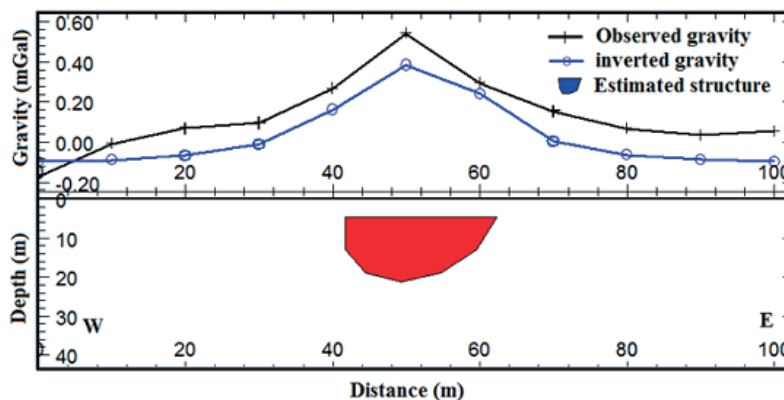


Figure 22. 2-D non-linear inverse modeling in the direction of profile AA'.

present study in revealing the underground anomaly source mass border was investigated with two synthetic models. The results indicate that density distributions obtained from the reweighting focusing inversion algorithm are well focused on the top part of the subsurface structure edges with the highest distance. Thus, by the use of this method, the underground depth and location of the farthest edges of an underground structure can be detected.

The inversion method was used for the analysis of the gravity horizontal gradient of a chromite mass. The density distributions estimated a depth of 5 meters for the eastern edge and 5 to 10 meters for the western edge of the subsurface mass, which are approximately similar to the results obtained by the non-linear inverted modeling (Figure 22). Three common edge detection filters were used for validation, which estimated the horizontal expansion of subsurface mass to compare with the value obtained from the inversion (26 meters). The conventional depth estimation methods have estimated the depth of the top surface of the chromite mass in the range between 5 to 10 meters. Therefore, the location of the subsurface density distributions is almost correspondent to the top surface of the mass. Also according to the results, it can be concluded that the highest horizontal expansion belongs to the top surface of the mass. The non-linear inverse modeling also estimated the expansion of the top surface of the subsurface mass about 21 meters which show a good conformity with the obtained result from the proposed method. It should be noted that the analyses made for the depth and expansion evaluation of the underground mass are related to the direction of the data sampling profile.

The use of the method developed in the present study, alongside other qualitative and quantitative maps, can effectively help the analyzer with the analysis of the gravity field and detection of the parameters of the underground structure.

Note: The quality of the images is the responsibility of the author.

9. References

- Aghajani H. (2013). Conducting survey and gravimetric studies on the eastern chromite zone of Sabzevar. Research project, Faculty of Mining, Petroleum and Geophysics Engineering, Shahrood University of Technology.
- Alp H., Albora A.M., Tur H. (2011). A view of tectonic structure and gravity anomalies of Hatay Region southern Turkey using wavelet analysis. *Journal of Applied Geophysics*, 75(3), 498-505. doi: <https://doi.org/10.1016/j.jappgeo.2011.07.004>
- Baroz J., Macaudiere J., Montigny R., Noghreyan M., Ohnenstetter M., Rocci G.A. (1984). Ophiolites and related formations in the central part of the Sabzevar (Iran) and possible geotectonic reconstructions. *Neues Jahrbuch für Geologie und Paläontologie, Abhandlungen*, 168(2-3), 358-388. doi: <https://doi.org/10.1127/njgpa/168/1984/358>
- Cooper G.R.J; Cowan D.R. (2006), Enhancing potential field data using filters based on the local phase. *Computers & Geosciences*, 32(10), 1585-1591. doi: <https://doi.org/10.1016/j.cageo.2006.02.016>
- Cooper G.R.J. (2009). Balancing images of potential-field data. *Geophysics*, 74(3), L17-L20. doi: <https://doi.org/10.1190/1.3096615>
- Cooper G.R.J., Cowan D.R. (2011). A generalized derivative operator for potential field data. *Geophysical Prospecting*, 59(1), 188-194. doi: <https://doi.org/10.1111/j.1365-2478.2010.00901.x>
- Eshaghzadeh A., Dehghanpour A., Kalantari R.S. (2018). Application of the tilt angle of the balanced total horizontal derivative filter for the interpretation of potential field data. *Bollettino di Geofisica Teorica ed Applicata*, 59(2), 161-178. doi: <https://doi.org/10.4430/bgta0233>
- Eshaghzadeh A., Hajian A. (2018). 2-D inverse modeling of residual gravity anomalies from Simplegeometric shapes using Modular Feed-forward Neural Network. *Annals of Geophysics*, 61(1), SE115. doi: <https://doi.org/10.4401/ag-7540>
- Eshaghzadeh A., Dehghanpour A., Kalantari R.S. (2019). Fault Strike Detection Using Satellite Gravity Data Decomposition by Discrete Wavelets: A Case Study from Iran. *Journal of Sciences, Islamic Republic of Iran*, 30(1), 41-50. doi: <https://doi.org/10.22059/jscienc-es.2019.69631>
- Eshaghzadeh A., Kalantari R.S. (2017). Canny edge detection algorithm application for analysis of the potential field map. *Earth Science India*, 10(3), 108-125.
- Eshaghzadeh A, Sahebari SS (2020) Application of PSO Algorithm based on the mean value of maximum frequency distribution for 2-D inverse modeling of gravity data due to a finite vertical cylinder shape. *Quaderni di Geofisica*, 162, 1-22. doi: <https://doi.org/10.13127/qdg/162>
- Eshaghzadeh A., Hajian A. (2020). Modelling of Residual Gravity Data due to a Near Surface Dyke Structure Using Damped SVD and Marquardt Inverse Methods. *Geofísica Internacional*, 61(4), 325-350. doi: <https://doi.org/10.22201/igeof.00167169p.2022.61.4.2203>
- Ferreira F.J.F., de Castro L.G., Bongiolo A.B.S., de Souza J., Romeiro M.A.T. (2011). Enhancement of the total horizontal gradient of magnetic anomalies using tilt derivatives: Part II—Application to real data. 81st Annual International Meeting, SEG, Expanded Abstracts. 887-891.
- Ferreira F.J.F., de Souza J.A.B.S., Bongiolo de Castro L.G. (2013). Enhancement of the total horizontal gradient of magnetic anomalies using the tilt angle. *Geophysics*, 78(3), J33-J41. doi: <https://doi.org/10.1190/geo2011-0441.1>
- Gerkense A.J.C. (1989). *Foundation of exploration Geophysics*. Elsevier.
- Görgün E., Albora A.M. (2017). Seismotectonic investigation of Biga Peninsula in SW Marmara Region using steerable filter technique, potential field data, and recent seismicity. *Pure and Applied Geophysics*, 174, 3889-3904. doi: <https://doi.org/10.1007/s00024-017-1604-0>
- Hou Z.L., Wei X.H., Huang D.N. (2015). Fast Density Inversion Solution for Full Tensor Gravity Gradiometry Data *Pure and Applied Geophysics*, 173(2), 509-523. doi: <https://doi.org/10.1007/s00024-015-1129-3>

- Li Y., Oldenburg D.W. (1996). 3-D inversion of magnetic data. *Geophysics*, 61(2), 394–408. doi: <https://doi.org/10.1190/1.1443968>
- Ma G., Li L. (2012). Edge detection in potential fields with the normalized total horizontal derivative. *Computers & Geosciences*, 41, 83–87. doi: <https://doi.org/10.1016/j.cageo.2011.08.016>
- Mehanee S., Golubev N., Zhdanov M.S. (1998). Weighted regularized inversion of the magnetotelluric data. *Society of Exploration Geophysicists*, 481–484. doi: <https://doi.org/10.1190/1.1820468>
- Miller H.G., Singh V. (1994). Potential field tilt—a new concept for the location of potential field sources. *Journal of Applied Geophysics*, 32(2-3), 213–217. doi: [https://doi.org/10.1016/0926-9851\(94\)90022-1](https://doi.org/10.1016/0926-9851(94)90022-1)
- Nabighian M.N. (1972). The analytic signal of two-dimensional magnetic bodies with polygonal cross-section: Its properties and use for automated anomaly interpretation. *Geophysics*, 37(3), 507–517. doi: <https://doi.org/10.1190/1.1440276>
- Nabighian M.N. (1974). Additional comments on the analytic signal of two-dimensional magnetic bodies with polygonal cross-section. *Geophysics*, 39(1), 85–92. doi: <https://doi.org/10.1190/1.1440416>
- Oldenburg D.W., Li Y. (2005). 5 Inversion for applied geophysics: A tutorial. *Investigations in geophysics*, 13, 89–150. doi: <https://doi.org/10.1190/1.9781560801719.ch5>
- Pilkington M. (1997). 3-D magnetic imaging using conjugate gradients. *Geophysics*, 62(4), 1132–1142. doi: <https://doi.org/10.1190/1.1444214>
- Portniaguine O., Zhdanov M.S. (1999). Focusing geophysical inversion images. *Geophysics*, 64(3), 874–887. doi: <https://doi.org/10.1190/1.1444596>
- Portniaguine O., Zhdanov M.S. (2002). 3-D magnetic inversion with data compression and image focusing. *Geophysics*, 67(5), 1532–1541. doi: <https://doi.org/10.1190/1.1512749>
- Rezaie M., Moradzadeh A., Nejati A., Aghajani M. (2016). Fast 3D focusing inversion of gravity data using reweighted regularized Lanczos Bidiagonalization method. *Pure and Applied Geophysics*, 174(1), 359–374. doi: <https://doi.org/10.1007/s00024-016-1395-8>
- Shamsipour P., Marcotte D., Chouteau M. (2012). 3D stochastic joint inversion of gravity and magnetic data. *Journal of Applied Geophysics*, 79, 27–37. doi: <https://doi.org/10.1016/j.jappgeo.2011.12.012>
- Tai-Han W., Da-Nian H., Guo-Qing M., Zhao-Hai M., Ye L. (2017). Improved preconditioned conjugate gradient algorithm and application in a 3D inversion of gravity-gradiometry data. *Applied Geophysics*, 14, 301–313. doi: <https://doi.org/10.1007/s11770-017-0625-x>
- Tian Y., Ke K., Wang Y. (2018). A Folding Calculation Method Based on the Preconditioned Conjugate Gradient Inversion Algorithm of Gravity Gradient Tensor. *Pure and Applied Geophysics*, 176, 215–234. doi: <https://doi.org/10.1007/s00024-018-1965-z>
- Tikhonov A.N., Arsenin V.Y. (1977). *Solution of Ill-Posed Problems*. V. H. Winston and Sons.
- Verduzco B., Fairhead J.D., Green C.M., Mackenzie C. (2004). New insights into magnetic derivatives for structural mapping. *The Leading Edge*, 23(2), 116–119. doi: <https://doi.org/10.1190/1.1651454>
- Wijns C., Perez C., Kowalczyk P. (2005). Theta map: Edge detection in magnetic data. *Geophysics*, 70(4), L39–L43. doi: <https://doi.org/10.1190/1.1988184>
- Yuan Y., Danian H., Qinglu Y., Pengyu L. (2014). Edge detection of potential field data with improved structure tensor methods. *Journal of Applied Geophysics*, 108, 35–42. doi: <https://doi.org/10.1016/j.jappgeo.2014.06.013>
- Zhen-Long H., Da-Nian H., En-De W., Hao C. (2019). 3D density inversion of gravity gradiometry data with a multilevel hybrid parallel algorithm. *Applied Geophysics*, 16, 141–152. doi: <https://doi.org/10.1007/s11770-019-0763-4>